Ileal proteomic changes associated with IL-25-mediated resistance against intestinal trematode infections

María Álvarez-Izquierdo
Universitat de Valencia
J. Guillermo Esteban
Universitat de Valencia
Carla Muñoz-Antoli
Universitat de Valencia
Rafael Toledo (rafael.toledo@uv.es)
https://orcid.org/0000-0003-2651-9794

Research

Keywords: proteomics, intestine, interleukin-25, intestinal helminths, trematoda, Echinostoma caproni

Posted Date: April 9th, 2020

DOI: https://doi.org/10.21203/rs.3.rs-21824/v1

Version of Record: A version of this preprint was published on July 2nd, 2020. See the published version at https://doi.org/10.1186/s13071-020-04206-y.

Abstract

Background: *Echinostoma caproni* (Trematoda: Echinostomatidae) is an intestinal trematode, which has been widely employed to investigate the factors determining the rejection of intestinal helminths. In this sense, several studies have shown that IL-25 is essential for the development of resistance against *E. caproni* in mice. In fact, treatment of mice with recombinant IL-25 generates resistance against primary *E. caproni* infection. However, the mechanisms by which IL-25 induces resistance remain unknown.

Methods: To study the mechanisms responsible for resistance elicited by IL-25, we analyze the ileal proteomic changes induced by IL-25 in mice and their potential role in resistance. To this purpose, we compare the protein expression profiles in the ileum of four experimental groups of mice: naïve controls; *E. caproni*-infected mice; rIL-25-treated mice; and rIL-25-treated mice exposed to *E. caproni* metacercariae.

Results: Quantitative comparison by 2D-DIGE showed significant changes in a total of 41 spots. Forty of those spots validated protein spots were were identified by mass spectrometry corresponding to 24 proteins.

Conclusions: The analysis of differentially expressed proteins indicates that maintenance of the intestinal epithelial homeostasis and the regulation of proliferation and cell death are the most affected processes that appears to be related to the resistance to infection. These results provide new insights into the proteins involved in the regulation of tissue homeostasis after intestinal infection and its transcendence in resistance.

Background

Intestinal helminth infections are highly prevalent parasitic diseases affecting more than one billion people worldwide, especially in developing regions of Asia, Africa and Latin America [1]. These infections are the cause of high morbidity, with most common symptoms related to effects on nutrition that may induce malabsorption syndrome, vitamin deficiencies, growth retardation or impaired cognitive function among other disorders. Additional complications such as intestinal obstruction, chronic dysentery, rectal prolapse, anemia or debilitating disease can appear [2–3]. Besides its interest in human health, helminth infections in livestock cause significant economic losses, directly by decreased productivity, or due to the indirect costs of anthelmintic treatment [4]. Among the intestinal helminth infections, those caused for trematodes constitute a major group of diseases that affects both humans and animals [5]. Intestinal trematodes are a large group of parasites and about seven million people are infected worldwide [6]. About 76 of species belonging to 14 families have been recorded infecting humans. Infection commonly occurs when humans eat raw or undercooked foods that contain the infective metacercariae. A variety of aliments are involved in the transmission of intestinal flukes and the eating habits are essential to determine the distribution of these parasitic diseases. High incidence of intestinal trematodiasis is strongly associated with populations living near freshwater bodies and the practice of eating raw or undercooked aquatic products [5]. One of the most relevant group of trematodes causing human infections, mainly in East and Southeast Asia, are the members of the family Echinostomatidae. Echinostomes are cosmopolitan parasites that infect a large number of different warm-blooded hosts, both in nature. More than 20 species belonging to nine genera of Echinostomatidae are known to cause human infections around the world [5]. Apart from their interest in human health echinostomes, and particularly *Echinostoma caproni*, have been extensively used as experimental models to the study of helminth-vertebrate host relationships, with emphasis in the factors determining resistance to intestinal helminth infections. *E. caproni* is an intestinal trematode with no tissue phases in the definitive host. After infection, the metacercariae excyst in the duodenum and the juvenile worms migrate to the ileum, where they attach to the mucosa [7]. *E. caproni* has a wide range of definitive hosts, although its compatibility differs considerably between rodent species on the basis of worm survival and development [7]. In mice and other hosts of high compatibility, the infection becomes chronic, while in hosts of low compatibility, (such as rats) the worms are expelled from the 2–4 weeks post-infection (wpi) [8–9].

In recent years, IL-25, a member of the IL-17 family of cytokines also called IL-17E, has been considered a key cytokine. IL-25 promotes Th2 immunity and exerts anti-inflammatory functions via the downregulation of Th17 and Th1 responses [10–12]. IL-25 expression is generally associated with resistance to gastrointestinal helminth infections through the activation of Th2 responses that mediate effector mechanisms for parasite expulsion (which include mast cell hyperplasia, smooth muscle hypercontractility, expression of RELM-β, and intestinal mastocytosis, amongst others) [13]. Intestinal tuft cells are the main source of IL-25. Upon helminth establishment, tuft cells release IL-25. In response to alarmins, group 2 of innate lymphoid cells (ILC2) produce large amounts of IL-13 that activates dendritic cells in the lamina propria and license their migration to mesenteric lymph nodes to polarize naïve CD4 + T cells into Th2. ILC2 and basophils can also perform antigen presentation to CD4 + T cells and induce Th2 polarization, which is aided by IL-4 in the case of basophils. Th2-polarized cells release an array of cytokines that drive effector mechanisms and expand themselves through positive feedback loops, amplifying the response and determining resistance to infection [13].

Previous studies of our group have shown that IL-25 is essential for the resistance to *E. caproni* infections and the susceptibility of mice relies on the inability of this host species to produce IL-25 in response to infection [14–15]. Susceptibility of mice to primary *E. caproni* infection was associated with low levels of intestinal IL-25 expression, whilst deworming via administration of praziquantel (pzq) was accompanied by a steady increase in IL-25 expression and, in turn, by the onset of a Th2-type response that prevented the establishment of secondary infections [14–15]. Although these facts, little is known about the mechanism by which IL-25 generates resistance against intestinal helminths. In the present work, we analyze the changes in the production of proteins induced by IL-25 in the ileum of mice that may be involved in the generation of resistance against intestinal helminths.

Materials And Methods

Animal and infection procedures

Thew present study was performed using a total of 15 male ICR (CD1) mice weighing 30–35 g. The *E. caproni* strain and the infection procedures carried out has been previously described [9, 16]. Briefly, encysted metacercariae were removed from kidneys and periacardial cavities of experimentally infected

Biomphalaria glabrata snails and used for infection. Mice were randomly allocated into four groups (3 mice in each group). Animals belonging to one of the groups were infected by gastric gavage with 50 metacercariae of *E. caproni*. Mice of a second group were treated with rIL-25 (R&D Systems®) (concentration: 0.2 µg/µl each) in 150 µl of PBS during each of the four days prior to infection with 50 metacercariae of *E. caproni* as described above. Animal of another group were simply treated with penicillin under the conditions described above. This group was not exposed to metacercariae of *E. caproni*. Finally, the remainder 5 mice were used as control and they were not exposed neither to rIL-25 nor *E. caproni* metacercariae. All mice were necropsied one week after the exposure to metacercariae of the first two groups of mice. The animals were maintained under standard conditions with food and water *ad libitum*.

Intestinal epithelial cells isolation and protein extraction

Ileal sections from mice in each group were removed at necropsy and IECs were isolated as described before [Muñoz-Antoli et al., 2014]. In brief, the intestinal sections were opened longitudinally and rinsed by gentle shaking in washing buffer: ice-cold Hank's balance salt solution (HBSS) containing 2% of heat-inactivated fetal calf serum (FCS). Supernatant was then removed and fresh washing buffer was added to the ileal sections. This step was repeated at least 4 times, until the supernatant was clear. The tissue was then cut into small, 1 cm-long, segments and incubated for 20 min at 37 °C in HBSS containing 10% FCS, 1 nM EDTA, 1 mM DTT, 100 U/ml penicillin and 100 µg/ml streptomycin (dissociation buffer). The supernatant was collected and maintained on ice and the incubation was repeated a second time with fresh dissociation buffer. Supernatants were combined and filtered through a 100 nm cell strainer before IECs were pelleted out by centrifuging at 200 g for 10 min at 4 °C and washed three times in PBS under the same centrifuge conditions to remove any residual medium.

Protein extraction was performed using M-PER Mammalian Protein Extraction Reagent (Thermo Scientific) according to the manufacturer's instructions. Shortly, extraction reagent was added to the IECs pellet (20:1, v/v), mixed by vortex and incubated at room temperature (RT) for 20 min under continuous gentle agitation. The lysate was then clarified by centrifugation at 18,000 g for 15 min at 4 °C, transferred into a new tube and stored at -80 °C until use.

Preparation of biological replicates and protein labeling

In order to increase the biological significance and avoid erroneous conclusions due to individual variations, four biological replicates were prepared for each experimental group: infected infected with *E. caproni*, rIL-25-treated mice exposed to *E. caproni* metacercariae, rIL-25-treated mice and naïve animals.

Three of this replicas were obtained from different animals and the fourth was obtained by mixing the previous three by applying the same amount of protein from each sample (20 µg/sample). Then, 200 µg of protein from each biological replicate were cleaned and precipitated with 2-D Clean-Up kit (GE Healthcare) to remove salts and other substances that interfere with labeling and electrophoresis. The samples were resuspended in DIGE tagged buffer (7M urea, 2 M tiourea, 4% CHAPS, 20 mM Tris). The protein concentration after precipitation was determined by the RC DC (BioRad Protein Assay) method, using BSA as standard protein. The concentrations for labeling with fluorochromes should be between 1 and 20 µg / µl, being between 5–10 µg / µl the optimum concentrations for labeling according to the manufacturer's instructions. With the precipitated samples, 100 µg pools needed for the experiment were made for each group, with equimolar amounts of each samples in each group and quantified again.

The DIGE experiment was designed to perform 8 gels containing the samples of the four groups to be compared. After checking that the pH of all samples was between 8 and 8.5, the CyDye DIGE Fluor (GE Healthcare®) fluorochromes were labeled according to the protocol recommended by the manufacturer.

In order to increase the biological significance and avoid erroneous conclusions due to individual variations, four biological replicates were prepared for each experimental group (control, infected, dewormed and reinfected). Each biological replicate was obtained by pooling the same amount (20 µg) of protein extracted from the IECs isolated from four different mice. Then, 50 µg of protein from each biological replicate were cleaned and precipitated with 2D Clean-up Kit (GE Healthcare), pellets were resuspended in 18 µl of a proper buffer (25 mM Tris, 7 M urea, 2 M thiourea, 4% CHAPS, pH 8,5) and proteins were fluorescently tagged with CyDye DIGE Fluor minimal dyes (GE Healthcare), following manufacturer's instructions. One microliter of dye (400 pmol) was added to each sample and maintained on ice for 30 min in the dark. The reaction was stopped by adding 1 µl of 10 mM lysine. To minimize any dye-specific labeling artefacts, two biological replicates of each experimental group were labeled with Cy3 and the other two were labeled with Cy5. The internal standard, prepared by mixing the same amount of protein of each sample included in the experiment, was always labeled with Cy2.

The proteomic analysis was performed in the proteomics facility of SCSIE University of Valencia. This proteomics laboratory is a member of Proteored, PRB3 and is supported by grant PT17/0019, of the PE I + D + i 2013–2016, funded by ISCIII and ERDF"

2D differential in gel electrophoresis (2D-DIGE)

To analyze the effect of IL-25 in the course of *E. caproni* infection, ileal protein extracts from naïve, infected, rIL-25-treated and rIL-25-treated and exposed to metacercariae mice were compared across 8 2D-DIGE to analize changes in the intestinal production of proteins. The 8 pairs of Cy3- and Cy5-labeled biological replicates (50 µg of protein each) were combined with a 50 µg aliquot of the Cy2-labeled internal standard. The mixtures containing 150 µg of protein were then separated in the first dimension, i.e. isoelectric focusing, and the second dimension. The IPG strips (24 cm, nonlinear pH 3–11) were rehydrated overnight with rehydration buffer (8 M urea, 4% CHAPS, 1% ampholytes and 12 µl/ml of DeStreak™), and the labeled samples were then applied to the strips by anodic cup loading, after the addition of DTT and ampholytes up to a final concentration of 65 mM and 1%, respectively. The isoelectric focusing was carried out at 20 °C in the Ettan IPGphor 3 System (GE Healthcare) as follows: (i) 300 V for 4 h; (ii) gradient to 1,000 V for 6 h; (iii) gradient to 8,000 V for 3 h; and (iv) 8,000 V up to 32,000 Vh. Prior to the second dimension the strips were equilibrated in two steps, 15 min each, in equilibration buffer (50 mM Tris, 6 M urea, 30% glycerol and 2% SDS) containing either 2% DTT or 2.5% iodoacetamide, respectively. The separation of proteins in the second dimension was performed on an Ettan DALTsix system (GE Healthcare) using 12.5% polyacrylamide gels. Electrophoresis was run at 1 W/gel for 1 h followed by 5 h, approximately, at 15 W/gel.

Imaging and 2D-DIGE analysis

Gels were scanned in a Typhoon™ 9400 Variable Mode Imager (GE Healthcare) at appropriate wavelengths for each fluorophore: Cy2 (488/520 nm), Cy3 (532/580 nm) and Cy5 (633/670 nm), and at 50 µm resolution. The non-essential information was removed using ImageQuant Tools software and DeCyder v7.0 software was employed for image analysis. The differential in gel analysis module was used for automatic spot detection and abundance measurements in each individual gel, comparing the normalized volume ratio of each spot from a Cy3- or Cy5-labeled sample to the corresponding Cy2 signal from the internal standard. Data sets were collectively analyzed using the biological variation analysis module of the same software, which allows inter-gel matching and calculation of standardized average volume ratios (AVRs) for each protein spot among the 8 gels of the study. Statistical analysis was assessed for each change in AVR using one-away ANOVA, along with the corresponding *post-hoc* analysis, and the false discovery rate (FDR) test, which avoids the introduction of false positives when performing multiple comparisons. Statistical significance was considered when $p < 0.01$ and $q < 0.05$ in the ANOVA and FDR analyses, respectively. Moreover, inter-gels matching of statistically different spots was confirmed manually.

Unsupervised principal components analyses (PCAs) and hierarchical clustering analyses (HCAs) (Euclidean) were performed using the DeCyder extended data analysis module, both on all protein spots present at least in 7 of the 8 gels of the experiment (85% presence) and the set of spots that were found to be significantly differentially expressed among the groups compared. These multivariate analyses group the individual biological replicates based on a collective comparison of the expression patterns of the set of proteins chosen, with any *a priori* knowledge of the biological reasons for clustering [17].

Mass spectrometry and protein identification

Spots showing significant changes in protein abundance among groups were manually excised from the gel and washed twice with double-distilled water. Thereafter, proteins were reduced in 100 mM ammonium bicarbonate containing 10 mM DTT for 30 min at 56 °C, alkylated with iodoacetamide 55mMin 100 mM ammonium bicarbonate for 20 min at RT in the dark and, finally, digested in-gel with an excess of sequencing grade trypsin (Promega) overnight at 37 °C, as described before [18]. Protein digestion was stopped with 1% TFA and peptides were dried in a vacuum centrifuge and resuspended in 7 µl of 0.1% TFA, pH 2. One microliter of peptide mixture was spotted onto a MALDI target plate and allowed to air dry at RT before adding 1 µl of matrix, a 5 mg/ml solution of α-cyano-4-hydroxy-transcinnamic acid (CHCA, Sigma-Aldrich®) in 0.1% TFA and 70% ACN, and left to air dry again.

Samples were analyzed in a 5800 MALDI TOF/TOF (AB Sciex) in positive reflectron mode using 3000 laser shots per position. Previously, the plate and the acquisition methods had been calibrated with 0.5 µl of CM5 calibration mixture (AB Sciex), in 13 positions. For the MS/MS analysis, 5 of the most intense precursors were selected for each position, according to the following threshold criteria: a minimum signal to-noise of 10; a minimum cluster area of 500; a maximum precursor gap of 200 ppmand amaximum fraction gap of 4.MS/MS data were acquired using the default 1 kV MS/MSmethod. Several spots could not be identified by MALDI TOF/TOF, however, LC-MS/MS was performed. Five microliters of each samplewere loaded onto a trap column:NanoLC Column, 3 µ C18-CL, 350 µm × 0.5 mm (Eksigen) and desalted with 0.1% TFA at 3 µl/min for 5 min. The peptides were then loaded onto an analytical column: LC Column, 3 µ C18-CL, 75 µm × 12 cm(Nikkyo), equilibrated with 5% ACN, 0.1% formic acid (FA). Elution was carried out with gradient of 5 to 45% B in A for 15 min (A: 0.1% FA; B: ACN, 0.1% FA) at a constant flow rate of 300 nl/min. Peptides were analyzed in a mass spectrometer nanoESI qQTOF (5600 TripleTOF, AB Sciex). The tripleTOF was operated in information-dependent acquisition mode, in which a 0.25-s TOF MS scan from m/z 350–1250 was performed, followed by 0.05-s product ion scans from m/z 100–1500 on the 50 most intense 2–5 charged ions.

Database search

Database search was performed using ProteinPilot v5.0. search engine (ABSciex). ProteinPilot default parameters were used to generate a peak list directly from 5600 TripleTof wiff files and Paragon algorithm of ProteinPilot v5.0 was employed to search in Uniprot database (versión 01-2017) with the following parameters: trypsin specificity, cys-alkylation, taxonomy restricted to human, and the search effort set to through. Identifications were accepted as positive when there were at least two different matching peptides (≥ 95% confidence) and ProteinPilot unused score was > 1.3, which means that proteins are identified with confidence ≥ 95%.

Results

Experimental infection with metacercariae of E. caproni and worm recovery

All the rIL-25-treated mice exposed to metacercariae became negative to infection at necropsy. In contrast all the non-treated mice exposed to metacercariae were positive to infection. The percentage of worms collected ranged from 40 to 100 (69.36 ± 16.29).

Analysis of protein production profiles by 2D-DIGE

A 2D-DIGE proteomic analysis was performed on whole ileal cell extracts from 16 biological replicates, corresponding to 4 experimental groups (4 replicates each) referred as: control, rIL-25-treated mice, rIL-25-treated mice exposed to metacercariae and infected mice. 2D-images were subjected to computational analysis using the DeCyder software and both multivariate and univariate analysis were applied to identify (i) the similarity in intestinal protein production profiles among experimental groups and (ii) particular differences in protein abundance between each group with respect to the others (Fig. S1).

The inter-gel spot matching revealed a total of 172 well defined spots with 85% of presence, found in at least 7 of the 8 gels that compromise the experiment. The average abundance of each spot among the 24 images of our study was calculated and significant differences were considered when $p < 0.01$, both in one-way ANOVA as well as in the post-hoc analysis. Results of the 2D-DIGE analysis are showed in Fig. 1.

Multivariate statistics: principal component and cluster analysis

Multivariate statistics allows the evaluation of the whole data set, conferring a biological interpretation of the results, which is based on the integral protein production profile of samples. PCAs and CAs between groups were carry out on the 172 spots with 85% of presence in the experiment and the 41 validated spots displaying significant differences among groups, with $p < 0.01$ in one-way ANOVA. In the three cases, both PCAs and CAs were compared two by two: one including biological replicates from control and rIL25-treated mice, other including biological replicates from rIL25-treated mice and rIL25-treated mice exposed to metacercariae and, finally, a third including biological replicates infected and rIL25-treated mice exposed to metacercariae. In the PCAs, appear the data cluster according the experimental condition where we can observe highlighted, spots with greater presence in one group with respect to the other. Likewise, CAs grouped the spots according to how similar their expression profile are between compaired experimental groups. Hence, according to multivariate statistical analyses, the 4 experimental groups were reduced to three comparative interest groups: 1) Infected animals vs rIL-25-treated animals; 2) rIL-25-treated mice exposed to metacercariae vs rIL-25-treated animals; and 3) naïve controls vs rIL-25-treated mice (Figs. 2–4).

One-way ANOVA and post-hoc analysis

A total of 59 differential spots (34.3%) were found, all of them displaying $q < 0.05$ in the FDR test. To ensure the proper comparison of spots among gels, the correspondence of these 59 spots were manually validated through all the gels, and 41 were unambiguously confirmed (Figs. 1 and S1).

Differentially identified spots were up- or downregulated (5 and 24, respectively) in the ileum of rIL-25-treated mice with respect rIL-25-treated animals and infected mice (4 and 1, respectively). Moreover, we found 7 spots differentially identified between maïve controls and rIL-25-treated mice from which 2 of them were up-regulated and the remainder 5 spots became downregulated. Details of the computational comparison of differential spots are compiled in Table S1 for non-similar groups (i.e. naïve controls vs. rIL-25-treated animals exposed to metacercariae and rIL-25-treated mice vs. infected animals).

Identification of differentially produced proteins

A total of 40 validated spots (5 upregulated and 24 downregulated in rIL-25-treated animals exposed to metacercariae vs rIL-25-treated mice; 4 upregulated and 1 downregulated in rIL-25-treated animals exposed to metacercariae vs infected mice; 2 upregulated and 5 downregulated in rIL-25-treated mice vs naïve animals) were accurately identified by MS and database search (Fig. 1). This 40 spots corresponded to 24 different proteins, since 6 of them were identified in more than one protein spot. These redundancies can be attributed to different post-translational modifications, the existence of isoforms or to protein modifications during samples preparation. Identified proteins are classified in Tables 1–3 according to their function, indicating for each spot if its production was up or downregulated due to inoculation of rIL25 in presence and/or ausence of *E. caproni* infection in mice. Differentially identified proteins were classified in: metabolic enzymes, structural proteins, antioxidant and detoxifying enzymes, calcium-binding proteins and cell regulation proteins.

Table 1

Proteins identified by 2D-DIGE/mass spectrometry as differentially expressed between intestinal epithelial cells of Infected mice versus rIL-25-treated animals exposed to metacerariae of *Echinostoma caproni*. MW: molecular weight; Cyt: cytoplasmatic; PM: plasma membrane.

Spot	Protein	Species	Expression	MW (kDa) Expected/observed	Isoelectric point Expected/observed	Cellular role	Location	Score	Coverage (%)	Pept
	Metabolic enzymes									
133	Enolase 1B	*Mus musculus*	-1.4	47/116	6.37/6.37	Glycolysis Plasminogen activation Ornithine metabolism	Cyt PM Mit	45.44	66.59	8
146	Enolase 1B	*Mus musculus*	+ 1.9	47/112	6.37/7.17	Glycolyis Plasminogen activation Ornithine metabolism	Cyt PM Mit	38.54	45.16	112
148	Enolase 1B	*Mus musculus*	+ 2.0	47/111	6.37/6.67	Glicolisis Plasminogen activation Ornithine metabolism	Cyt PM Mit	108.86	87.33	176
273	Glyceraldehyde-3-phosphate dehydrogenase	*Mus musculus*	+ 2.4	35/93	8.44/8.44	Glycolysis	Cyt	32.38	62.76	29
291	Lactate dehydrogenase	*Mus musculus*	+ 1.5	36/88.8	7.61/9.26	Pyruvate fermentation to lactate	Cyt	16.31	45.48	29

Table 3

Proteins identified by 2D-DIGE/mass spectrometry as differentially expressed between intestinal epithelial cells of rIL-25-treated mice versus rIL-25-treated a exposed to metacerariae of *Echinostoma caproni*. MW: molecular weight; Cyt: cytoplasmatic; PM: plasma membrane; Mit: mitochondrion; Nuc: nucl

Spot	Protein	Species	Expression	MW (kDa) Expected/observed	Isoelectric point Expected/observed	Cellular role	Location	Score	Coverag (%)
	Metabolic enzymes								
63	Pyruvate Kinase PKM	*Mus musculus*	-1.9	58/132	7.17/8.20	Glycolysis	Cyt Nuc	51.34	52.54
69	Pyruvate Kinase PKM	*Mus musculus*	-1.7	58/132	7.17/8.48	Glycolysis	Cyt Nuc	46.03	42.94
101	Glutamate dehydrogenase 1	*Mus musculus*	-1.6	61/126	8.05/8.05	Glutamine anaplerosis	Mit	70.19	62.54
123	6-Phodphogluconate dehydrogenase	*Mus musculus*	-1.7	53/122	6.81/7.62	Pentose phosphate pathway	Cyt	14	18.84
144	Enolase 1B	*Mus musculus*	-1.8	47/118	6.37/8.46	Glycolysis	Cyt PM Mit	89.91	79.95
154	Fumarate hydratase	*Mus musculus*	-1.6	54/118	9.12/9.12	Krebs cycle	Mit	39.41	35.5
156	Enolase 1B	*Mus musculus*	-1.8	47/118	6.37/6.37	Glycolysis	Cyt PM Mit	46.26	51.15
166	Creatine kinase B-type	*Mus musculus*	-2.0	43/116	5.34/5.34	Cretine kinase activity	Cyt	12.4	29.92
184	Phosphoglycerate kinase 1	*Mus musculus*	-2.3	45/114	8.02/9.5	Glycolysis	Cyt	46.01	63.55
214	Glyceraldehyde-3-phosphate dehydrogenase	*Mus musculus*	-1.9	36/108	8.44/9.43	Glycolysis	Cyt	15.03	42.94
226	Aspartate aminotransferase	*Mus musculus*	-2.2	47/108	9.13/9.92	Aminoacid metabolism	Mit	48.42	50
250	Transaldolase	*Mus musculus*	-1.8	42/102	6.57/7.04	Pentose phosphate pathway	Cyt	20.35	35.34
257	Malate dehydrogenase	*Mus musculus*	-1.8	37/96	6.16/6.16	Krebs Cycle	Cyt	28.05	41.62
262	Glyceraldehyde-3-phosphate dehydrogenase	*Mus musculus*	+ 1.8	36/100	8.44/8.44	Glycolysis	Cyt	13.22	39.64
279	Ornithine carbamoyltransferase	*Mus musculus*	-2.0	39/100	8.81/8.30	Ornithine metabolism	Mit	35.79	45.87
290	Palmitoyl-protein thioesterase	*Mus musculus*	-2.6	35/94	8.26/8.85	Palmitoyl metabolism	Cyt	10,04	21.5
296	Malate dehydrogenase	*Mus musculus*	-1.8	37/94	6.16/6.28	Krebs Cycle Malate shuttle	Cyt	61.69	74.55
302	Malate dehydrogenase	*Mus musculus*	+ 2.2	37/90	6.16/5.58	Krebs Cycle Malate shuttle	Cyt	17.01	36.53
305	Malate dehydrogenase	*Mus musculus*	+ 1.7	37/90	6.16/5.98	Krebs Cycle Malate shuttle	Cyt	42.04	53.59
387	Triosephosphate isomerase	*Mus musculus*	-1.8	32/60	5.56/8.66	Glycolysis Gluconeogenesis	Cyt	3.9	16.03
	Structural proteins								
243	Junction plakoglobin	*Mus musculus*	-2.3	82/104	5.75/6.43	Cell adhesión	Cyt	39.85	46.98
260	Junction plakoglobin	*Mus musculus*	-1.5	82/102	5.75/8.18	Cell adhesion	Cyt	29.38	29.4
325	Junction plakoglobin	*Mus musculus*	-1.6	82/86	5.75/6.34	Cell adhesion	Cyt	12.5	17.85

Spot	Protein	Species	Expression	MW (kDa) Expected/observed	Isoelectric point Expected/observed	Cellular role	Location	Score	Coverag (%)
	Antioxidant-detoxifying enzymes								
358	Dihydropteridine reductase	*Mus musculus*	-2.5	22/74	7.67/8.40	Oxireductase activity	Mit	11.8	31.92
418	Glutathione S-transferase P 1	*Mus musculus*	-1.6	24/60	7.69/8.33	Glutathione conjugation and detoxification	Cyt Mit Nuc	18.06	57.14
421	Glutathione S-transferase P 1	*Mus musculus*	-1.7	24/59	7.69/9.21	Glutathione conjugation and detoxification	Cyt Mit Nuc	31.38	78.1
431	Peroxiredoxin-1	*Mus musculus*	-2.0	22/57	8.26/8.26	Redox regulation	Cyt	10.18	33.67
	Calcium-binding proteins								
271	Annexin A2	*Mus musculus*	+ 1.6	39/101	7.55/8.84	Membrane transport Fibrin homeostasis	PM	39.75	71.98
324	Annexin A4	*Mus musculus*	+ 2.5	36/86	5.43/5.02	Membrane transport	PM ext.	23.72	41.69

Table 3

Proteins identified by 2D-DIGE/mass spectrometry as differentially expressed between intestinal epithelial cells of naïve control mice versus rIL-25-treated anin

Cyt: cytoplasmatic; PM: plasma membrane; Mit: mitochondrion; Nuc: nucleus.

Spot	Protein	Species	Express.	MW (kDa) Expected/observed	Isoelectric point Expected/observed	Cellular role	Location	Score
	Metabolic enzymes							
144	Enolase 1B	*Mus musculus*	+ 1.2	47/110	6.37/6.37	Glycolysis Plasminogen activation Ornithine metabolism	Cyt PM Mit	89.91
147	Enolase 1B	*Mus musculus*	-1.5	47/110	6.37/6.75	Glycolysis Plasminogen activation Ornithine metabolism	Cyt PM Mit	37.45
533	Triosephosphate isomerase	*Mus musculus*	-1.9	32/60	5.56/6.28	Glycolysis Gluconeogenesis	Cyt	25
	Structural proteins							
527	Junction plakoglobin	*Mus musculus*	+ 1.7	82/27	5.75/8.70	Cell adhesion	Cyt	3.33
	Antioxidant-detoxifying enzymes							
404	Peroxiredosin-4	*Mus musculus*	-1.9	31/60	6.67/5.90	Redox regulation	Cyt	10.61
	Cell regulation proteins							
159	Proliferation-associated 2G4	*Mus musculus*	-1.8	50/108	6.41/6.83	Apoptotic process Cell diferentiation	Cyt Nuc 29.09	41.62	16
306	Receptor of activated protein C kinase 1	*Mus musculus*	-1.8	35/83	7.6	Apoptotic process Biological rhythms Translation regulation	PM Nuc 13.62	27.76	7

Discussion

Recent studies of our group showed that partial resistance against *E. caproni* secondary infections is developed after chemotherapeutic cure of a primary infection and innately produced IL-25 is crucial to determine the resistance. Susceptibility to primary infections was associated with low levels of intestinal IL-25 expression, whilst deworming via administration of praziquantel was accompanied by a steady increase in IL-25 expression that prevented the establishment of secondary infections [14–15]. However, it is not well defined if the participation of IL-25 in resistance to infection. Herein, we analyze the proteomic changes indiced by IL-25 that may contribute to resistance to infection.

Resistance against *E. caproni* infection has been associated with the preservation of the intestinal homeostasis despite the possible damage induced by the parasite. In resistant hosts, *E. caproni* infection elicits a rapid renewal of the intestinal that allows to maintain the epithelium homeostasis and impairing the proper worm establishment. In contrast, in susceptible hosts, such as mice, the development of chronic infections are related to the disruption of the intestinal homeostasis causing tissue hyperplasia [19–21]. Although mice is a susceptible host, treatment with rIL-25 prior to infection induces complete resistance to the infection [15]. Our results support that IL-25 may contribute to resistance by the enhancement of intestinal homeostasis via activation of the canonical wingless-related integrator site (Wnt)/β-Catenin signaling pathway. Treatment of naïve mice with rIL-25 only elicited changes in the production of a total of 5 proteins, including the structural protein junction plakoglobin or γ-catenin. This protein is a member of the catenin family, paralog to β-catenin, and is a component of desmosomes. It is involved in the mechanisms of cell adhesion and is essential to maintain and regulate intestinal epithelial homeostasis [22–24]. Plakoglobin participates in the canonical pathway of Wnt/β-Catenin signaling since elevated levels of plakoglin promote the stabilization and nuclear localization of β-catenin enhancing the activation of Wnt/β-Catenin signaling [25]. Activation of this pathway is essential for the maintenance of the intestinal homeostasis since it plays an essential role in regulating cell proliferation, survival, and differentiation facilitating epithelial healing after disruption [26]. The central mediator of Wnt signaling is β-catenin. Wnt signaling activation is dependent on the nuclear translocation of β-catenin. When a canonical Wnt binds to the frizzled receptor and its co-receptor lipoprotein receptor-related protein 5/6, dishevelled is recruited and the destruction complex is inhibited, thus promoting the accumulation of non-phosphorylated β-catenin in the cytosol. As non-phosphorylated β-catenin accumulates intracellularly, it is translocated to the nucleus where it activates the T-cell factor/lymphocyte enhancer factor transcription factor families to regulate gene transcription [27]. Plakoglobin participates in the canonical pathway of Wnt/β-Catenin signaling since this protein inhibits the glycogen synthase kinase (GSK3β)-mediated nuclear localization of β-catenin. GSK-3β is one important member that regulates the Wnt/β-catenin target gene expression by controlling the level of cytoplasmic β-catenin and its nuclear shuttle [28]. Elevated levels of plakoglin promote the stabilization and nuclear localization of β-catenin [25] and may enhance intestinal homeostasis despite the damage caused by the infection. Oudhoff and co-workers [29] reported that Wnt/β-Catenin signaling is an important component of resistance to the intestinal nematode *Trichuris muris* in mice. These authors showed that Wnt expression programs are induced upon infection with *T. muris* eggs and wild type mice were able to expel the infection. In contrast, mice deficient in SETD7 (a member of the Suppressor of variegation 3-9-Enhancer of zeste-Trithorax domain-containing family of lysine methyltransferases) were not able to reject the infection. SETD7 controls IEC turn over by modulating developmental signaling pathway Wnt/β-Catenin. Lack of SETD7 resulted in downregulation of Wnt/β-catenin, deficient and susceptibility to infection [29]. The fact exposure of rIL-25-treated mice to *E. caproni* metacercariae induced a significant downregulation of three isoforms of plakoglobin with respect to rIL-25-treated mice supports that plakoglobin plays an important role in *E. caproni* infections and its potential role in the development of resistance to infection.

Strikingly, two other proteins involved in cell differentiation and tissue homeostasis also became altered by the treatment with rIL-25. Proliferation-associated 2G4 [PA2G4) and receptor of activated protein C kinase 1 (RACK1) were found to be downregulated in rIL-25-treated mice with respect to naïve mice. PA2G4, also known as EBP1, is a RNA-binding protein that is involved in growth regulation. This protein is present in pre-ribosomal ribonucleoprotein complexes and may be involved in ribosome assembly and the regulation of intermediate and late steps of rRNA processing. This protein can interact with the cytoplasmic domain of the ErbB3 receptor and may contribute to transducing growth regulatory signals. This protein is also a transcriptional corepressor of androgen receptor-regulated genes and other cell cycle regulatory genes through its interactions with histone deacetylases. This protein has been implicated in growth inhibition [30–31]. The EBP1-binding in promoters regulated by E2F can result in an enhanced ability of EBP1 to suppress genes transcription regulated by the cell cycle and inhibit cell growth [30, 32]. Furthermore, the expression of EBP1 generates the negative expression of the androgen receptor (AR) and several of its target genes, thereby inhibiting AR-regulated cell growth [30–33]. RACK1 is a member of the tryptophan-aspartate repeat (WD-repeat) family of proteins and shares significant homology to the β subunit of G-proteins (Gβ). RACK1 adopts a seven-bladed β-propeller structure which facilitates protein binding. RACK1 has a significant role to play in shuttling proteins around the cell, anchoring proteins at particular locations and in stabilizing protein activity. It interacts with the ribosomal machinery, with several cell surface receptors and with proteins in the nucleus. As a result, RACK1 is a key mediator of various pathways and contributes to numerous aspects of cellular function. RACK1 is a scaffolding protein that takes part in the maintenance of intestinal homeostasis protecting the integrity of the epithelial barrier by suppressing the regeneration and proliferation of crypt cells, promotes differentiation and apoptosis and is generated against stress responses [34–36]. Downregulation of both EBP1 and RACK1 may contribute to prevent the hyperplasia in the intestinal tissue that is associated to susceptibility to *E. caproni* infections.

Another striking feature that may be related with alterations in the intestinal epithelium and resistance to infections is in the upregulation of annexins 2 and 4 min rIL-25-treated mice exposed to *E. caproni* metacercariae.. Annexin is a common name for a family of structurally related proteins that mostly found in eukaryotic organisms both in extra and intracellular environment and bind phospholipids and carbohydrates in the presence of Ca^{2+} [37–38]. Annexins play a role in the control of cell death and affect membrane properties such as permeability or anchoring of cytoskeletal elements [39–40]. These proteins also are related to epithelial cell migration that is a critical event in gastrointestinal mucosal wound healing [41] Furthermore, evidences of annexins as modulators of inflamation have been widely provided [42]. In the small intestine, the expression of annexins appears to be restricted to M cells, where it plays a role in endocytic transport and membrane scaffolding [43]. Annexins can function as a natural ligand for phosphatidylserine, a prominent phospholipid that is exposed during cell death. It has been suggested that annexins blocks posphatidylserine-dependent phagocytosis of dying cells, forcing its internalization and delivering phosphatidylserine back to the inner leaflet of the cell membrane [44]. Annexins have been implicated in the repair mechanisms on both tissue and intracelular levels [40]. Upregulation of annexins has been reported in association with resistance to *E. caproni* secondary infections in mice [38]. This was

attributed to the reduced rate of cell death that happens despite induction of mitochondrial dysfunction, cellular senescence and high levels of oxidative stress [38].

Specifically, annexin 4 appears to play a specific role in membrane repair. Plasma membrane repair mechanisms involve internalization via endocitosis, or exocytosis as observed from mechanical wounding or exposure to plasma membrane poreforming agents [45–48]. Therefore, overexpression of annexin 4 due to the exposurte to metacercariae of rIL-25-treated mice may contribute to the defense of this parasite infection participating in the healing of the intestinal tissue and acting as an anti-inflammatory factor. Annexin 2 is a protein that is part of the lipid rafts in the intestinal brush border and is associated with actin filaments mediating in membrane-membrane and membrane-cytoskeletal interactions influencing actin cytoskeletal remodeling through targeting signaling molecules to membrane domains. As a consequence it plays an important role in membrane trafficking and stabilization of membrane-associated protein complexes with the actin cytoskeleton and has been implicated in the migration of various cell types including epithelial cells and cell matrix interaction [41, 49]. Moreover, annexin 2 has been shown to induce clustering of specific plasma membrane phospholipids and play a role in lipid domain formation [41]. The absence of annexin 2 would therefore influence RhoA-mediated F-actin reorganization, which in turn affects motility of annexin 2 defficient cells [41]. In this sense, our results suggest that the up-regulation of both annexins (annexin 2 and 4) could help maintain the epithelial barrier structure during helminth infections.

Quantitatively, the proteins involved in metabolic processes were the most altered in any of the groups studied. A generalized reduction of ileal cell metabolism has been observed at 2 weeks after *E. caproni* infection in presence of rIL-25. A total of twenty of the identified spots (corresponding to 15 different proteins) are metabolic enzymes and a great part of them were significantly downregulate in infected in presence of rIL-25 mice with respect to control inoculated with rIL-25. Alterations in several proteins involved in the Krebs cycle (fumarate hydratase and malate dehydrogenase) and in the pentose phosphate pathway (transaldolase and 6-phosphogluconate dehydrogenase). We also detected a reduced expression of several glycolytic enzymes including several isoforms of enolase 1B, glyceraldehyde-3-phosphate dehydrogenase and pyruvate kinase PKM, phosphoglycerate kinase 1 and triosephosphate isomerase. This may indicate mitochondrial dysfunction and a subsequent decrease in aerobic metabolism as a consequence of the exposure to *E. caproni* metacercariae. A similar situation has been described in the ileum of *E. caproni* mice at 2 wppi [21]. The reduction of aerobic metabolism was associated with an increase in the anaerobic use of glucose, through the overexpression of lactate dehydrogenase. However, Cortés and co-workers [38] detected a marked downregulation of the production of lactate dehydrogenase were in the ileum of resistant secondarily infected mice, suggesting that both aerobic and anaerobic metabolism become impaired as the infection progresses. In contrast, in our study, lactate dehydrogenase was upregulated in the ileum of rIL-25-treated mice exposed to the infection with respect to mice conventionally infected. This might indicate that infection requires an increase in the anaerobic use of glucose to supports the high energy demand caused by parasitic infection both presence/absence of rIL-25 to cover the metabolic demand generated by mitochondrial dysfunction. The impact that alterations in energy metabolism has over the course of the infection is difficult to assess according to our current knowledge. However, it could be of relevance for a better understanding of the mechanisms developed in the intestinal environment in responses to helminth infections.

Several antioxidant and detoxifying enzymes such as peroxiredoxins 1 and 4, glutathione S-transferase and dihydropteridine reductase were also found to be altered. Treatment with rIL-25 induced a marked downregulation of peroxiredoxin 4. This enzyme is a ubiquitously expressed member of the peroxiredoxin family that is localized in the endoplasmic reticulum and extracellular space [52]. Peroxiredoxin 4 diminishes oxidative stress by reducing hydrogen peroxide to water in a thiol-dependent catalytic cycle and has been linked to the regulation of the key pro-inflammatory transcription factor, nuclear factor kappa B (NF-κB) [53–55]. This supports that the processes related to oxidative stress and cell death are altered in the presence of infection by *E. caproni* independently of the presence and IL-25. IL-25 does not appear to take part in the regulation of the processes related to oxidative stress and apoptosis necessary to maintain intestinal homeostasis. Strikingly, exposure of rIL-25-treated mice to metacercariae caused a downregulation of peroxiredoxin 1 instead peroxiredoxin 4. Peroxiredoxin 1 plays a key role against reactive oxygen species and antioxidants and in in inflammatory responses [56]. The production of this enzyme is upregulated in active ulcerative colitis specimens, and it increases along with the inflammation level in ulcerative colitis regenerative mucosal crypt epithelial cells [57–58]. Downregulation of peroxiredoxin 1 was observed as a consequence of the curation of an *E. caproni* infection [38]. The reduced production of this enzyme after infection in presence of rIL-25 may play a double role, promoting crypt-cell proliferation but, at the same time, inducing oxidative stress and ROS-mediated programmed cell death to counteract homeostatic dysregulation induced by the infection [21, 59–60].

Infection of rIL-25-treated mice also induced reduction in the production of palmitoyl-protein thiosterase (PPT). Protein thioestherases, or depalmitoylases, mediate the depalmitoylation of modified proteins, thereby completing a cycle of this reversible post-translational modification [61–63]. Palmitoylation can effectively act as a post-translational “switch” on some proteins and provide dynamic control over protein localization or function. Indeed, palmitoylation plays critical roles in protein trafficking and strongly influences the stability of proteins [64–69]. PPT1 is a lysosomal substrate that enter in the lysosome via autophagy leading to signaling of several processes related with anabolic and catabolic metabolism in the cell [63, 70]. PTT deficiency has been implicated in the disruption of the lysosome-endosomal pathway and in other cellular processes, including endocytosis, vesicular trafficking, synaptic function, lipid metabolism, neural specification, and axon connectivity and seems to be involved in cell susceptibility to apoptotic cell death and defects in the mitochondrial enzyme activities and adaptive energy metabolism [71]. For this reason, Downregulation of PPT after exposure to *E. caproni* metacercariae presence of rIL-25 mice may be due to its role in processses regulation involved in cell death and energy metabolism in order to maintain intestinal homeostasis. This is supported by the concomitant downregulation of creatine kinase B-type (CKB). This enzyme plays a critical role in energy transduction in tissues with increases in energy demands. The creatine kinase energy system is itself further regulated by hypoxic signaling and can enhance creatine metabolism during oxygen deprivation to promote tissue healing and homeostasis [72]. Impaired Cr/PCr shuttling may contribute to dysregulated mitochondrial energetics and an increased barrier permeability characteristic of inflamed mucosa ans susceptibility to *E. caproni* infection [9, 21, 73].

Conclusions

Our results indicate that IL-25 and the *E. caproni* infection in presence of IL-25 induce proteomic changes in the ileum of mice that may contribute to resistance to infection. The main groups of proteins that become altered were those involved in the preservation and healing of the epithelial architecture

enhancing the maintenance of the epithelium. Considering altogether our results, the maintenance of the intestinal homeostasis seems to be essential for resistance to infection. Our study provides new insights into the proteins involved in the regulation of tissue homeostasis in the presence of rIL-25, a cytokine that is considered as a target factor for the development of resistance to intestinal helminths.

Declarations

Author contributions

MAI and RT carried out the experiments designed the experiments and wrote the manuscript. CMA and JGE analyzed the data and revised the manuscript. RT was the principal investigator for the project and was responsible for project design, statistical analysis, and article writing.

Funding

This work was supported by Ministerio de Economía y Competitividad (Madrid, Spain) (grant number: BFU2016-75639-P) and from Ministerio de Sanidad y Consumo (Madrid, Spain) (No. RD12/0018/0013, Red de Investigación Cooperativa en Enfermedades Tropicales – RICET, IV National Program of I+D+I 2008-2011, ISCIII – Subdirección General de Redes y Centros de Investigación Cooperativa and FEDER).

Availability of data and materials

Not applicable.

Ethics statements

This study was approved by the Ethical Committee of Animal Welfare and Experimentation of the University of Valencia (Ref#A18348501775). Protocols adhered to Spanish (Real Decreto 53/2013) and European (2010/63/UE) regulations.

Consent for publication

Not applicable.

Competing interests

The authors declare that they have no competing interests.

References

1. Gazzinelli-Guimaraes PH, Nutman TB. Helminth parasites and immune regulation. F1000Res. 2018; 7:1685. doi: 10.12688/f1000research.15596.1
2. Nokes C, Bundy DA. Does helminth infection affect mental processing and educational achievement? Parasitol Today 1994; 10:14-8.
3. Bethony J, Brooker S, Albonico M, Geiger SM, Loukas A, Diemert D, et al. Soil-transmitted helminth infections: ascariasis, trichuriasis, and hookworm. Lancet. 2006; 367:1521-32.
4. Hotez PJ, Alvarado M, Basáñez MG, Bolliger I, Bourne R, Boussinesq M, et al. The global burden of disease study 2010: interpretation and implications for the neglected tropical diseases. PLoS Negl Trop Dis. 2014; 8:e2865. doi: 10.1371/journal.pntd.0002865
5. Toledo R, Alvárez-Izquierdo M, Muñoz-Antoli C, Esteban JG. Intestinal trematode infections. Adv Exp Med Biol. 2019; 1154:181-213. doi: 10.1007/978-3-030-18616-6_7
6. Fürst T, Keiser J, Utzinger J. Global burden of human food-borne trematodiasis: a systematic review and meta-analysis. Lancet Infect Dis. 2012; 12:210-21. doi: 10.1016/S1473-3099(11)70294-8
7. Toledo R, Esteban JG, Fried B. Recent advances in the biology of echinostomes. Adv Parasitol. 2009; 69:147-204. doi: 10.1016/S0065-308X(09)69003-5
8. Toledo R, Espert A, Carpena I, Muñoz-Antoli C, Fried B, Esteban JG. The comparative development of *Echinostoma caproni* (Trematoda: Echinostomatidae) adults in experimentally infected hamsters and rats. Parasitol Res. 2004; 93:439-44
9. Muñoz-Antoli C, Sotillo J, Monteagudo C, Fried B, Marcilla A, Toledo R. Development and pathology of *Echinostoma caproni* in experimentally infected mice. J Parasitol. 2007; 93:854–89. doi: 10.1645/GE-1091R.1
10. Owyang AM, Zaph C, Wilson EH, Guild KJ, McClanahan T, Miller HR, et al. Interleukin 25 regulates type 2 cytokine-dependent immunity and limits chronic inflammation in the gastrointestinal tract. J Exp Med. 2006; 203:843-9
11. Kleinschek MA, Owyang AM, Joyce-Shaikh B, Langrish CL, Chen Y, Gorman DM, Blumenschein WM, McClanahan T, Brombacher F, Hurst SD, Kastelein RA, Cua DJ. IL-25 regulates Th17 function in autoimmune inflammation. J Exp Med. 2007; 204:161-70.
12. Liu DL, Zhao LX, Zhang S, Du JR. Peroxiredoxin 1-mediated activation of TLR4/NF-κB pathway contributes to neuroinflammatory injury in intracerebral hemorrhage. Int Immunopharmacol. 2016; 41:82-9. doi: 10.1016/j.intimp.2016.10.025
13. Cortés A, Muñoz-Antoli C, Esteban JG, Toledo R. Th2 and Th1 responses: clear and hidden sides of immunity against intestinal helminths. Trends Parasitol. 2017; 33:678-93. doi: 10.1016/j.pt.2017.05.004
14. Muñoz-Antoli C, Cortés A, Martin-Grau C, Fried B, Esteban JG, Toledo R. Partial resistance to homologous challenge infections of the digenean *Echinostoma caproni* in ICR mice. J Helminthol. 2016; 90: 428-33. doi: 10.1017/S0022149X1500053X

15. Muñoz-Antoli C, Cortés A, Santano R, Sotillo J, Esteban JG, Toledo R. Interleukin-25 induces resistance against intestinal trematodes. Sci Rep. 2016; 6:34142. doi: 10.1038/srep34142
16. Fujino T, Fried B. *Echinostoma caproni* and *E. trivolvis* alter the binding of glycoconjugates in the intestinalmucosa of C3H mice as determined by lectin histochemistry. J Helminthol. 1993; 67:179–88.
17. Silva TS, Richard N, Dias JP, Rodrigues PM. Data visualization and feature selection methods in gel-based proteomics. Curr Protein Pept Sci. 2014; 15:4–22. doi: 10.2174/1389203715666140221112334
18. Shevchenko A, Tomas H, Havlis J, Olsen JV, Mann M. In-gel digestion for mass spectrometric characterization of proteins and proteomes, Nat Protoc. 2006; 1:2856-60.
19. Muñoz-Antoli C, Cortés A, Sotillo J, Fried B, Esteban JG, Toledo R. Differential expression and glycosylation of proteins in the rat ileal epithelium in response to *Echinostoma caproni* infection. J Proteomics. 2014; 101:169-78. doi: 10.1016/j.jprot.2014.02.014
20. Cortés A, Muñoz-Antoli C, Sotillo J, Fried B, Esteban JG, Toledo R. *Echinostoma caproni* (Trematoda): differential in vivo mucin expression and glycosylation in high- and low-compatible hosts. Parasite Immunol. 2015; 37:32-42. doi: 10.1111/pim.12159
21. Cortés A, Sotillo J, Muñoz-Antoli C, Fried B, Esteban JG, Toledo R. Altered protein expression in the ileum of mice associated with the development of chronic infections with *Echinostoma caproni* (Trematoda). PLoS Negl Trop Dis. 2015; 9:e0004082. doi: 10.1371/journal.pntd.0004082
22. Yin T, Getsios S, Caldelari R, Kowalczyk AP, Müller EJ, Jones JC, et al. Plakoglobin suppresses keratinocyte motility through both cell-cell adhesion-dependent and -independent mechanisms. Proc Natl Acad Sci U S A. 2005; 102:5420-5
23. Aktary Z, Bertrand JU, Larue L. The WNT-less wonder: WNT-independent β-catenin signaling. Pigment Cell Melanoma Res. 2016; 29:524-40. doi: 10.1111/pcmr.12501
24. Fevr T, Robine S, Louvard D, Huelsken J. Wnt/beta-catenin is essential for intestinal homeostasis and maintenance of intestinal stem cells. Mol Cell Biol. 2007; 27:7551-9
25. Morgan RG, Pearn L, Liddiard K, Pumford SL, Burnett AK, Tonks A, et al. γ-Catenin is overexpressed in acute myeloid leukemia and promotes the stabilization and nuclear localization of β-catenin. Leukemia. 2013; F27:336-43. doi: 10.1038/leu.2012.221
26. Qian J, Huang X, Zhang Y, Ye X, Qian W. γ-Catenin Overexpression in AML Patients May Promote Tumor Cell Survival via Activation of the Wnt/β-Catenin Axis. Onco Targets Ther. 2020; 13:1265-1276. doi: 10.2147/OTT.S23087
27. Ackers I, Malgor R. Interrelationship of canonical and non-canonical Wnt signalling pathways in chronic metabolic diseases. Diab Vasc Dis Res. 2018; 15:3-13. doi: 10.1177/1479164117738442
28. Jacobs KM, Bhave SR, Ferraro DJ, Jaboin JJ, Hallahan DE, Thotala D. GSK-3β: A Bifunctional Role in Cell Death Pathways. Int J Cell Biol. 2012; 2012:930710. doi: 10.1155/2012/930710
29. Oudhoff MJ, Antignano F, Chenery AL, Burrows K, Redpath SA, Braam MJ, Perona-Wright G, et al. Intestinal Epithelial Cell-Intrinsic Deletion of Setd7 Identifies Role for Developmental Pathways in Immunity to Helminth Infection. PLoS Pathog. 2016; 12:e1005876. doi: 10.1371/journal.ppat.1005876
30. Zhang Y, Hamburger AW. Heregulin regulates the ability of the ErbB3-binding protein Ebp1 to bind E2F promoter elements and repress E2F-mediated transcription. J Biol Chem. 2004; 279:26126-33
31. Karlsson T, Altankhuyag A, Dobrovolska O, Turcu DC, Lewis AE. A polybasic motif in ErbB3-binding protein 1 (EBP1) has key functions in nucleolar localization and polyphosphoinositide interaction. Biochem J. 2016; 473:2033-47. doi: 10.1042/BCJ20160274
32. Lyne JC, Melhem MF, Finley GG, Wen D, Liu N, Deng DH, et al. Tissue expression of neu differentiation factor/heregulin and its receptor complex in prostate cancer and its biologic effects on prostate cancer cells in vitro. Cancer J Sci Am. 1997; 3:21–30.
33. Mamidipudi V, Cartwright CA. A novel pro-apoptotic function of RACK1: suppression of Src activity in the intrinsic and Akt pathways. Oncogene. 2009; 28: 4421-33. doi: 10.1038/onc.2009.293
34. Adams DR, Ron D, Kiely PA. RACK1, a multifaceted scaffolding protein: Structure and function. Cell Commun Signal. 2011; 9: 22. doi: 10.1186/1478-811X-9-22.
35. Duff D, Long A. Roles for RACK1 in cancer cell migration and invasion. *Cell Signal* 2017 35: 250-5. doi: 10.1016/j.cellsig.2017.03.005
36. Monastyrskaya K, Babiychuk EB, Draeger A. The annexins: spatial and temporal coordination of signaling events during cellular stress. Cell Mol Life Sci. 2009; 66:2623-42. doi: 10.1007/s00018-009-0027-1
37. Cortés A, Sotillo J, Muñoz-Antolí C, Martín-Grau C, Esteban JG, Toledo R. Resistance against *Echinostoma caproni* (Trematoda) secondary infections in mice is not dependent on the ileal protein production. J Proteomics. 2016; 140:37-7. doi: 10.1016/j.jprot.2016.03.034
38. Gerke V, Creutz CE, Moss SE. Annexins: linking Ca2+ signalling to membrane dynamics. Nat Rev Mol Cell Biol. 2005; 6:449-61
39. Gerke V, Moss SE. Annexins: from structure to function. Physiol Rev. 2002; 82:331-71.
40. Babbin BA, Parkos CA, Mandell KJ, Winfree LM, Laur O, Ivanov AI, et al. Annexin 2 regulates intestinal epithelial cell spreading and wound closure through Rho-related signaling. Am J Pathol. 2007; 170:951-66. doi: 10.2353/ajpath.2007.060647
41. Wallner BP, Mattaliano RJ, Hession C, Cate RL, Tizard R, Sinclair LK, et al. Cloning and expression of human lipocortin, a phospholipase A2 inhibitor with potential anti-inflammatory activity. Nature. 1986; 320:77–81.
42. Verbrugghe P, Waelput W, Dieriks B, Waeytens A, Vandesompele J, Cuvelier CA. Murine M cells express annexin V specifically. J Pathol. 2006; 209:240-9.
43. Kenis H, van Genderen H, Deckers NM, Lux PA, Hofstra L, Narula J, et al. Annexin A5 inhibits engulfment through internalization of PS-expressing cell membrane patches. Exp Cell Res. 2006; 312:719-26.
44. Steinhardt, R. A., Bi, G. & Alderton, J. M. Cell membrane resealing by a vesicular mechanism similar to neurotransmitter release. Science. 1994; 263:390–3.

45. Idone V, Tam C, Goss JW, Toomre D, Pypaert M, Andrews NW. Repair of injured plasma membrane by rapid Ca2+-dependent endocytosis. J Cell Biol. 2008; 180:905-14. doi: 10.1083/jcb.200708010
46. Corrotte M, Almeida PE, Tam C, Castro-Gomes T, Fernandes MC, Millis BA, et al. Caveolae internalization repairs wounded cells and muscle fibers. Elife. 2013; 2:e00926. doi: 10.7554/eLife.00926
47. Boye TL, Maeda K, Pezeshkian W, Sønder SL, Haeger SC, Gerke V,et al. Annexin A4 and A6 induce membrane curvature and constriction during cell membrane repair. Nat Commun. 2017; 8:1623. doi: 10.1038/s41467-017-01743-6.
48. Merrifield CJ, Rescher U, Almers W, Proust J, Gerke V, Sechi AS, et al. Annexin 2 has an essential role in actin-based macropinocytic rocketing. Curr Biol. 2001; 11:1136-41.
49. Grill D, Matos ALL, de Vries WC, Kudruk S, Heflik M, Dörner W, et al. Bridging of membrane surfaces by annexin A2. Sci Rep. 2018; 8:14662. doi: 10.1038/s41598-018-33044-3
50. Desrosiers RR, Gauthier F, Lanthier J, Béliveau R. Modulation of Rho and cytoskeletal protein attachment to membranes by a prenylcysteine analog. J Biol Chem. 2000; 275:14949-57.
51. Tavender TJ, Springate JJ, Bulleid NJ. Recycling of peroxiredoxin IV provides a novel pathway for disulphide formation in the endoplasmic reticulum. EMBO J. 2010; 29:4185-97. doi: 10.1038/emboj.2010.273
52. Wood ZA, Poole LB, Karplus PA. Peroxiredoxin evolution and the regulation of hydrogen peroxide signaling. Science. 2003; 300:650-3
53. Yu S, Mu Y, Ao J, Chen X. Peroxiredoxin IV regulates pro-inflammatory responses in large yellow croaker (*Pseudosciaena crocea*) and protects against bacterial challenge. J Proteome Res. 2010; 9:1424-36. doi:10.1021/pr900961x
54. Yanagisawa R, Warabi E, Inoue K, Yanagawa T, Koike E, Ichinose T, et al. Peroxiredoxin I null mice exhibits reduced acute lung inflammation following ozone exposure. J Biochem. 2012; 152:595-601. doi: 10.1093/jb/mvs113
55. Liu CH, Kuo SW, Hsu LM, Huang SC, Wang CH, Tsai PR, et al. Peroxiredoxin 1 induces inflammatory cytokine response and predicts outcome of cardiogenic shock patients necessitating extracorporeal membrane oxygenation: an observational cohort study and translational approach. J Transl Med. 2016; 14:114. doi: 10.1186/s12967-016-0869-x
56. Waage A, Brandtzaeg P, Halstensen A, Kierulf P, Espevik T. The complex pattern of cytokines in serum from patients with meningococcal septic shock. Association between interleukin 6, interleukin 1, and fatal outcome. J Exp Med. 1989; 169:333–8.
57. Zhao Y, Oberley TD, Chaiswing L, Lin SM, Epstein CJ, Huang TT, et al. Manganese superoxide dismutase deficiency enhances cell turnover via tumor promoter-induced alterations in AP-1 and p53-mediated pathways in a skin cáncer model. Oncogene. 2002; 21:3836-46.
58. Hu W, Chen SS, Zhang JL, Lou XE, Zhou HJ. Dihydroartemisinin induces autophagy by suppressing NF-κB activation. Cancer Lett. 2014; 343:239–48. doi: 10.1016/j.canlet.2013.09.035
59. Mizushima, N. Autophagy: process and function. *Genes Dev*. 2007 21:2861–2873.
60. Mizushima N, Komatsu M. Autophagy: renovation of cells and tissues. Cell. 2011; 147:728-41. doi: 10.1016/j.cell.2011.10.026
61. Koster KP, Yoshii A. Depalmitoylation by Palmitoyl-Protein Thioesterase 1 in Neuronal Health and Degeneration. Front Synaptic Neurosci. 2019; 11:25. doi: 10.3389/fnsyn.2019.00025
62. Dunphy J, Linder M. Signalling functions of protein palmitoylation. Biochim Biophys Acta. 1998; 1436, 245–261. doi: 10.1016/s0005-2760(98)00130-1
63. Linder ME, Deschenes RJ 2007. Palmitoylation: policing protein stability and traffic. Mol Cell Biol. 2007; 8:74–84. doi: 10.1038/nrm2084.
64. Fukata, Y, Fukata M. Protein palmitoylation in neuronal development and synaptic plasticity. *Nat Rev* Neurosci. 2010; 11:161–75. doi: 10.1038/nrn2788
65. Salaun C, Greaves J, Chamberlain L. The intracellular dynamic of protein palmitoylation. J Cell Biol. 2010; 191:1229–38. doi: 10.1083/jcb.201008160
66. Chamberlain LH, Lemonidis K, Sanchez-Perez M, Werno MW, Gorleku OA, Greaves J. Palmitoylation and the trafficking of peripheral membrane proteins. Biochem Soc Trans. 2013; 41:62-6. doi: 10.1042/BST20120243
67. Montersino A, Thomas GM. Slippery signaling: Palmitoylation-dependent control of neuronal kinase localization and activity. Mol Membr Biol. 2015; 32:179-88. doi: 10.1080/09687688.2016.1182652
68. Perera RM, Zoncu R. The lysosome as a regulatory hub. Annu Rev Cell De Biol. 2016; 32:223–53. doi: 10.1146/annurev-cellbio-111315- 125125
69. Kang, R, Wan J., Arstikaitis P, Takahashi H, Huang K., Bailey AO, et al. 2008. Neural palmitoyl-proteomics reveals dynamic synaptic palmitoylation. Nature. 2008; 456:904–9. doi: 10.1038/nature07605
70. Glykys J, Sims KB 2017. The neuronal ceroid lipofuscinosis disorders. In ed Swaiman KF, Ferreiro DM, Finkel RS, Pearl PL, Ashwal S, Schor NF, Gropman AL, Shevell MZ, editors. Swaiman's Pediatric Neurology (6th edition). Amsterdam: Elsevier; 2017., p. 390–404. doi: org/10.1016/B978-0-323-37101-8.00048-5
71. Mooseker, MS. Organization, chemistry, and assembly of the cytoskeletal apparatus of the intestinal brush border. Annu Rev Cell Biol. 1985; 1:209–41.
72. Toledo R, Monteagudo C, Espert A, Fried B, Esteban JG, Marcilla A. *Echinostoma caproni*: intestinal pathology in the golden hamster, a highly compatible host, and the Wistar rat, a less compatible host. Exp Parasitol. 2006; 112:164-71.

Figures

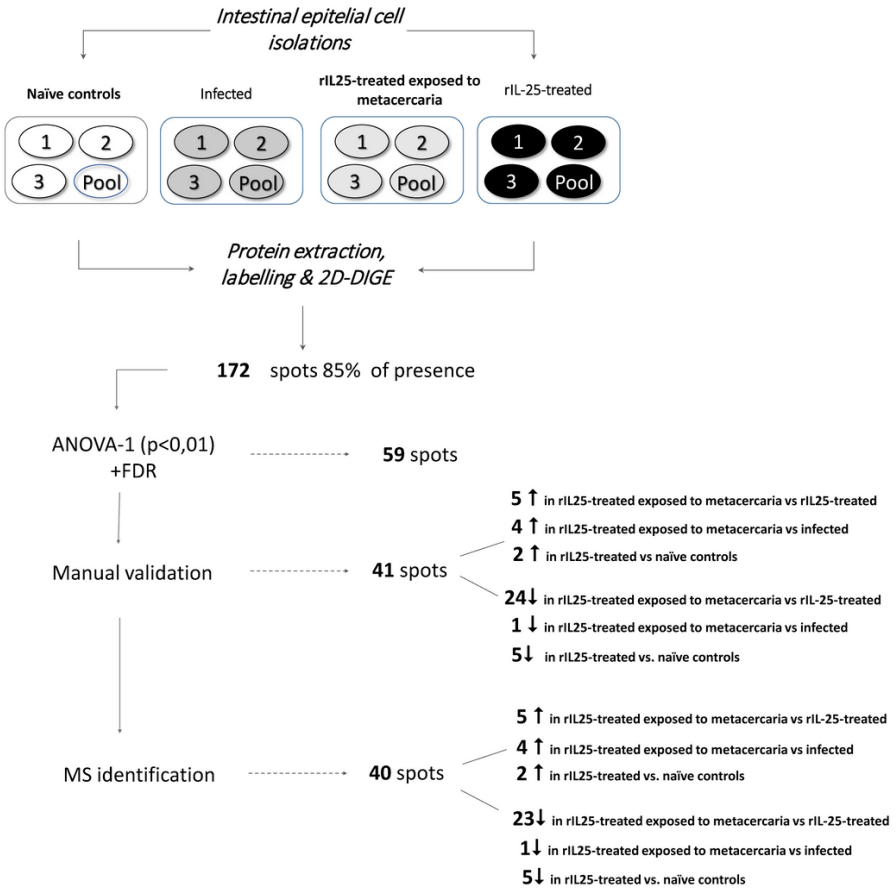

Figure 1

Schematic overview of results obtained by 2D-DIGE in the comparison of protein production profiles of intestinal epithelial cells isolated from naïve controls, rIL25-treated mice, infected animals and rIL25-treated mice exposed to metacercariae of Echinostoma caproni.

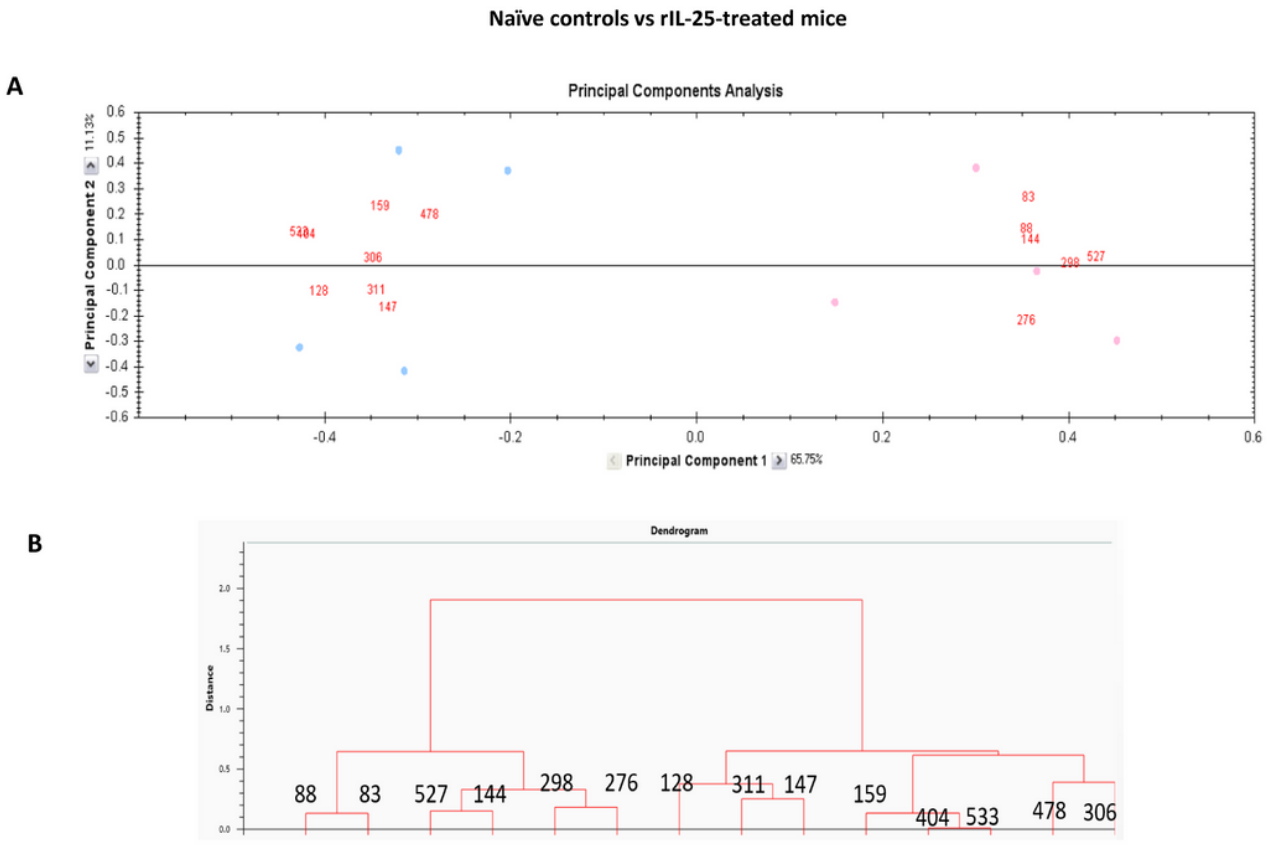

Figure 2

Multivariate statistical analysis applied to the set of 41 manually validated differential spots (85% of presence; $p < 0.01$; $q < 0.05$) in the 2D-DIGE experiment comparing naïve controls and rIL-25-treated mice: (A) plot from the principal components analysis between compared groups separated in two areas according to their overexpression in one group respect the other; (B) dendrogram from the hierarchical clustering analysis (Euclidean).

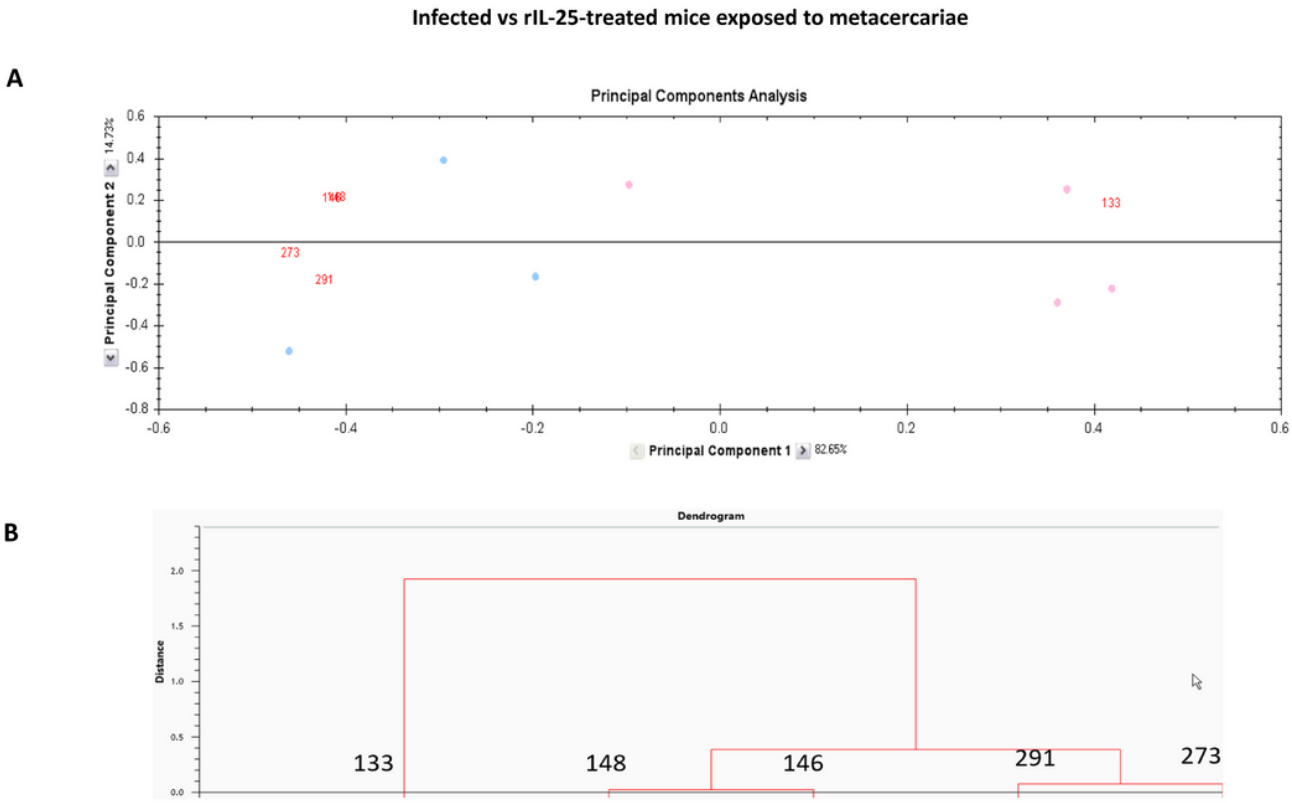

Figure 3

Multivariate statistical analysis applied to the set of 41 manually validated differential spots (85% of presence; $p < 0.01$; $q < 0.05$) in the 2D-DIGE experiment comparing infected vs rIL-25-treated mice exposed to Echinostoma caproni metacercariae: (A) plot from the principal components analysis between compared groups separated in two areas according to their overexpression in one group respect the other; (B) dendrogram from the hierarchical clustering analysis (Euclidean).

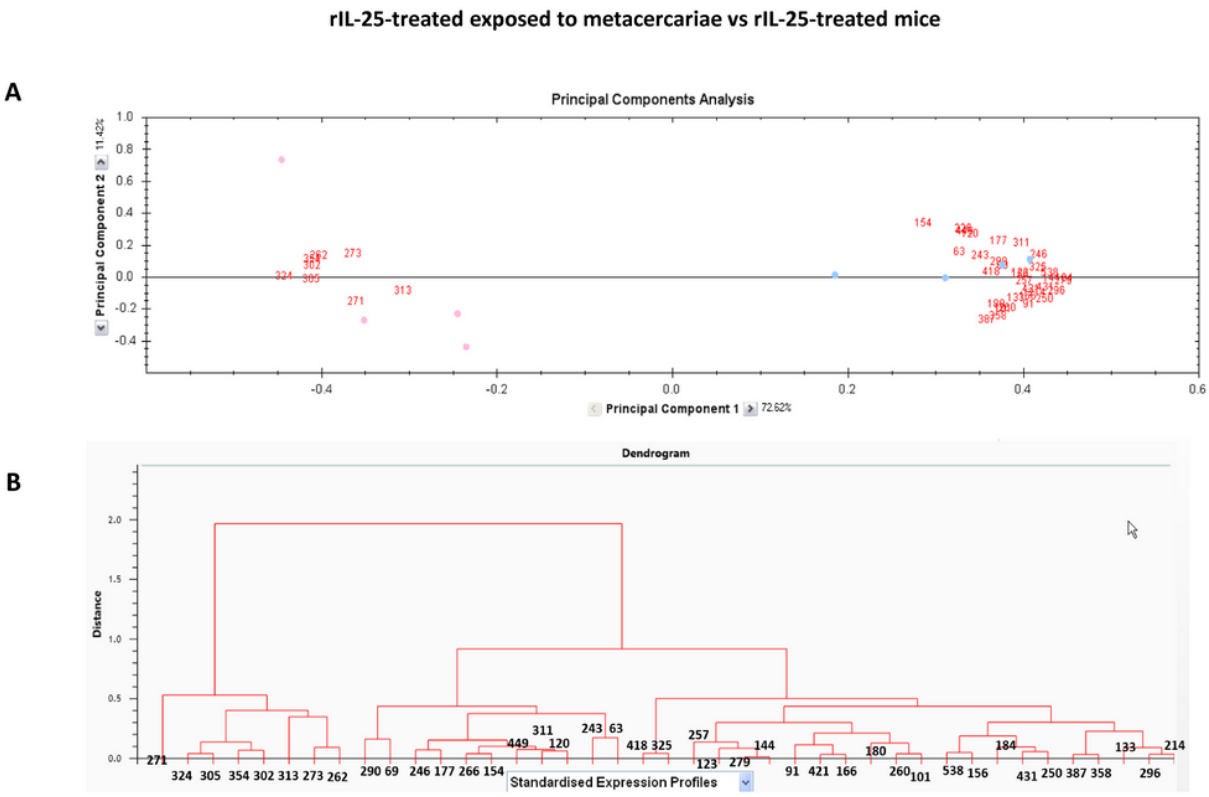

Figure 4

Multivariate statistical analysis applied to the set of 41 manually validated differential spots (85% of presence; $p < 0.01$; $q < 0.05$) in the 2D-DIGE experiment comparing rIL-25-treated exposed to Echinostoma caproni metacercariae vs rIL-25-treated mice: (A) plot from the principal components analysis between compared groups separated in two areas according to their overexpression in one group respect the other; (B) dendrogram from the hierarchical clustering analysis (Euclidean).

Supplementary Files

This is a list of supplementary files associated with this preprint. Click to download.

- GraphicalAbstract.jpg
- FigureS1.jpg
- TABLES1.pdf